Hindawi
Shock and Vibration
Volume 2021, Article ID 5536853, 12 pages
https://doi.org/10.1155/2021/5536853

Research Article

Study on the Unbalanced Fault Dynamic Characteristics of Eccentric Motorized Spindle considering the Effect of Magnetic Pull

Zhan Wang, Wenzhi He, Siyuan Du, and Zhe Yuan

School of Mechanical Engineering, Shenyang Jianzhu University, Shenyang, Liaoning 110168, China

Correspondence should be addressed to Zhe Yuan; yuanzhe@sjzu.edu.cn

Received 6 January 2021; Revised 21 February 2021; Accepted 11 March 2021; Published 26 April 2021

Academic Editor: Hui Ma

Unbalanced fault is the most common fault of high-speed motorized spindle, which is the main factor affecting the machining accuracy of high-speed spindle. Due to the unbalanced magnetic pull produced by the air gap eccentricity of the stator and rotor, the unbalanced vibration of the motorized spindle will be further aggravated. In order to explore the dynamic behavior and motion law of the unbalanced fault motorized spindle under the eccentric state, a dynamic model of the unbalanced fault of the high-speed motorized spindle considering the unbalanced magnetic pull was established. Taking the eccentric motorized spindle customized by the research group as the research object, the dynamic model is established, simulated, and analyzed, and the response change law of motorized spindle under the effect of different speed, unbalance, and air gap is obtained. The simulation results show that the unbalanced magnetic pull caused by static eccentricity will increase the unbalanced vibration of motorized spindle, and the unbalanced vibration will also increase with the increase of static eccentricity. The vibration caused by unbalanced magnetic pull does not increase with the increase of rotating speed. In frequency-domain analysis, when there is unbalanced magnetic pull, the peak appears at 0 Hz, and the amplitude of fundamental frequency vibration will increase with the increase of eccentricity. The experimental results show that the greater the eccentricity is, the greater the unbalance vibration of the motorized spindle is. The experimental results are consistent with the simulation results, which further verify the accuracy of the model. The research results lay a theoretical basis for fault analysis and diagnosis of coupling fault motorized spindle.

1. Introduction

In recent years, with the development of high-end manufacturing and processing in the direction of high speed and high precision, higher processing requirements have been put forward for high-end CNC machine tool. As the core component of CNC machine tools, the operation accuracy and performance of the motorized spindle unit are the key to high-speed and high-precision machining. During the operation of the motorized spindle, it will be subject to the coupling effect of the structure and the electromagnetic field. Due to installation errors and machining accuracy, the geometric center of the stator and rotor will have position eccentricity. Thus, the air gap distribution inside the motorized spindle is not uniform, which will lead to the result that unbalanced magnetic pull is generated; and unbalanced mass of the rotating spindle itself will also cause unbalanced vibration of the motorized spindle during operation. These will affect the machining accuracy of the motorized spindle and more seriously may cause equipment failure. To solve the unbalanced fault caused by the eccentricity of the motorized spindle and the position eccentricity of the stator and rotor is the key issue to improve the machining quality of the machine tool. So it is vital to deeply study the dynamic behavior of the unbalanced fault of the motorized spindle under eccentricity.

In recent years, the vibration and fault dynamics of rotors similar to motorized spindle have always been a research hotspot in the field of rotor vibration, and a large number of scholars have carried out in-depth research. Liu proposed an improved dynamic model for unbalanced high-speed motorized spindle considering the internal clearance

and air magnetic field energy [1]. Shi studied the orbit-spinning behaviors of the outer ring in a full ceramic ball bearing-steel pedestal system in wide temperature ranges [2, 3]. Shan et al. established a high-speed motorized spindle bearing-rotor dynamics model and analyzed the relationship between high speed and the transfer function of the milling cutter tip point [4]. Phadatare and Pratiher conducted a nonlinear dynamic analysis of a lightweight flexible rotor-disk-bearing system with geometric eccentricity and mass unbalance [5]. Wang and Jiang used Runge-Kutta method to successfully numerically solve the control equation of the dual-rotor system with unbalanced and unaligned coupling faults [6]. Qiao and Zhu studied the unbalanced vibration of the grinding wheel and provided a theoretical basis for dynamic balance [7]. Bab et al. studied the influence of mass eccentricity and surrounding medium damping on the steady-state response of the system [8]. Yue et al. found that mass eccentricity can increase the rotor vibration and weaken the influence of unbalanced magnetic pull and make the vibration tend to be regular [9]. Kong et al. studied the effect of mass eccentricity on the unbalanced response of induction motors through modeling [10]. Gao et al. studied the effect of unbalanced magnetic pull and mass eccentricity on the vibration of the motorized spindle but did not consider the influence of the gyro torque [11]. Faiz et al. proposed an analysis method that combines the concept of double penetration and superposition, which can predict the air gap magnetic field distribution of a surface-mounted permanent magnet motor with an eccentric air gap [12]. Xu et al. studied the nonlinear response of the rotor when the rotor is eccentric [13]. Tang et al. studied the stator vibration characteristics of the turbo generator under normal operating conditions and the combined fault of air gap eccentricity and rotor turn-to-turn short circuit [14]. Zuo et al. analyzed the excitation source using the finite element method and the effect of the unbalanced magnetic pull on the longitudinal dynamics evaluation index influences [15]. Liu et al. studied the mechanical coupling and magnetic coupling of permanent magnet synchronous motors [16]. Boy and Hetzler studied the lateral stability behavior and static torque characteristics of magnetic eccentricity [17]. Liu established a Jefferson rotor model considering the static radial eccentricity and studied the effect of unbalanced magnetic pull on the eddy of permanent magnet synchronous motors [18, 19]. Kumar and Kalita studied the causes and control methods of unbalanced magnetic pull [20]. Chen et al. studied the magnetic model of the motor [21]. Xiang et al. studied the influence of UMP on the nonlinear dynamic characteristics of permanent magnet synchronous motor rotor system [22]. Tang et al. analyzed the influence of radial air gap eccentricity on the radial unbalanced magnetic pull and vibration characteristics of the turbine generator rotor when the number of pole pairs is 1 [23]. Werner explained how to consider electromagnetic field damping when analyzing the forced vibration caused by eccentricity [24]. In summary, the research on rotor failure dynamics and vibration has formed a good theoretical basis. However, there are few studies on coupling faults mainly based on unbalanced magnetic pull between stator and rotor of motorized spindle. Therefore, it is of great significance to study the causes of unbalanced magnetic pull and its influence on rotor vibration.

In the above studies, most of the researches on air gap eccentricity to rotor bearing system are focused on motor. However, due to the complexity of the structure of motorized spindle, in particular the influence of unbalanced magnetic pull caused by eccentricity between stator and rotor on vibration cannot be ignored. With the increase of speed of motorized spindle, the operation stability of motorized spindle will be more affected, thus affecting the processing quality. In this paper, the expression of unbalanced magnetic pull of motorized spindle is derived first, and then a fault dynamic model of unbalanced magnetic pull coupling with mass eccentricity considering gyroscopic moment is established based on Lagrange method. The customized motorized spindle is taken as the research object to carry out simulation analysis. The influence of mass eccentricity, air gap eccentricity, and speed on the vibration characteristics of the spindle is discussed in detail. The research results of this paper provide certain theoretical reference for fault diagnosis, early prediction, and further dynamic balance regulation of coupled faulty motorized spindle.

2. Dynamic Modeling

2.1. The Mechanism of Unbalanced Magnetic Pull. The matching structure diagram of the motorized spindle stator and rotor is shown in Figure 1. There is a millimeter-level air gap between the rotor and stator. The main reason for unbalanced magnetic pull is the asymmetry of magnetic field between the stator and rotor, which leads to the asymmetry of magnetic pull force of rotor in radial direction, and unbalanced force produces force biased to one side. The uneven distribution of the air gap is the main reason for the uneven distribution of the magnetic field. When the geometric centers of the stator and rotor do not coincide, the uneven air gap around the rotor will occur; and because it is impossible to make the stator and rotor geometric center overlap even after rigorous testing and calibration, the unbalanced magnetic pull is inevitable.

2.2. Magnetic Pull Model of the Motorized Spindle. A brief diagram of static eccentricity of rotor section of motorized spindle is shown in Figure 2. The large circle represents the internal measurement of the stator, and the small circle represents the outside of the rotor. The air gap of the eccentric rotor can be approximately expressed as

$$\delta(\alpha, t) \approx \delta_0 - r\cos(\alpha - \gamma), \tag{1}$$

where δ_0 denotes the average air gap width of the motorized spindle, α and r denote the angle of any position and the static eccentric distance of the rotor, respectively, and γ denotes the static eccentric angle of the rotor.

The expression to expand the air gap into a series is

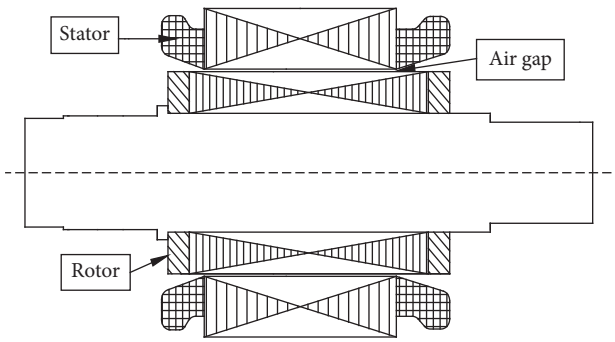

Figure 1: Motorized spindle diagram.

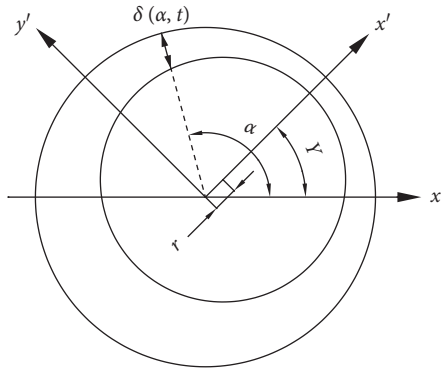

Figure 2: Rotor static eccentricity diagram.

$$\Lambda = \frac{\mu_0}{\delta} = \frac{\mu_0}{\delta_0 [1 - \varepsilon \cos(\alpha - \gamma)]} = \frac{\mu_0}{\delta_0} \sum_{n=0}^{\infty} \varepsilon^n \cos^n(\alpha - \gamma) = \sum_{n=0}^{\infty} \Lambda_n \cos n(\alpha - \gamma), \tag{2}$$

where $\varepsilon = (r/\delta_0)$ indicates relative eccentricity and μ indicates the air permeability coefficient.

Fourier Coefficient Λ_n is as follows:

$$\Lambda_n = \begin{cases} \dfrac{\mu_0}{\delta_0} \dfrac{1}{\sqrt{1-\varepsilon^2}}, & (n = 0), \\ \dfrac{2\mu_0}{\delta_0} \dfrac{1}{\sqrt{1-\varepsilon^2}} \left(\dfrac{1}{1 + \sqrt{1-\varepsilon^2}} \right)^n, & (n > 0). \end{cases} \tag{3}$$

The air gap fundamental magnetomotive force can be calculated by

$$F(\alpha, t) = F_j \cos(\omega t - p\alpha), \tag{4}$$

where p denotes the number of pole pairs of the motor, F_j denotes the fundamental magnetomotive force of the rotor exciting current, and ω denotes the electrical frequency.

The expression of the air gap distribution is

$$B = \mu_0 \frac{F}{\delta} = \Lambda(\alpha, t) F(\alpha, t), \tag{5}$$

Ignoring the smaller magnetic close component, the Maxwell stress of the normal component is

$$\sigma = \frac{B^2}{2\mu_0}. \tag{6}$$

The expression of the unbalanced magnetic pull can be derived by integrating the above formula on the rotor surface.

$$F_x = \begin{cases} f_1 \cos\gamma + f_2 \cos(2\omega t - \gamma) + f_3 \cos(2\omega t - 3\gamma) & p = 1, \\ f_1 \cos\gamma + f_3 \cos(2\omega t - 3\gamma) + f_4 \cos(2\omega t - 5\gamma) & p = 2, \\ f_1 \cos\gamma + f_4 \cos(2\omega t - 5\gamma), & p = 3, \\ f_1 \cos\gamma, & p > 3, \end{cases}$$

$$F_y = \begin{cases} f_1 \sin\gamma + f_2 \sin(2\omega t - \gamma) - f_3 \sin(2\omega t - 3\gamma), & p = 1, \\ f_1 \sin\gamma + f_3 \sin(2\omega t - 3\gamma) - f_4 \sin(2\omega t - 5\gamma), & p = 2, \\ f_1 \sin\gamma + f_4 \sin(2\omega t - 5\gamma), & p = 3, \\ f_1 \sin\gamma, & p > 3, \end{cases} \tag{7}$$

$$f_1 = \frac{RL\pi}{4\mu_0} F_j^2 (2\Lambda_0\Lambda_1 + \Lambda_1\Lambda_2 + \Lambda_2\Lambda_3),$$

$$f_2 = \frac{RL\pi}{4\mu_0} F_j^2 \left(\Lambda_0\Lambda_1 + \frac{1}{2}\Lambda_1\Lambda_2 + \frac{1}{2}\Lambda_2\Lambda_3 \right),$$

$$f_3 = \frac{RL\pi}{4\mu_0} F_j^2 \left(\Lambda_0\Lambda_3 + \frac{1}{2}\Lambda_1\Lambda_2 \right),$$

$$f_4 = \frac{RL\pi}{8\mu_0} F_j^2 \Lambda_2\Lambda_3,$$

where R represents the rotor radius, L represents the axis length, γ represents the static eccentricity angle, F_x and F_y represent the magnetic pull in x direction and in y direction, respectively, f_1, f_2, f_3, and f_4 represent the magnetic pull, respectively, and n represents the unbalanced tension series.

2.3. Dynamic Model. Due to manufacturing and material reasons, even if the motorized spindle rotor is dynamically balanced, there will still be unbalanced mass. These unbalanced masses will cause unbalanced vibration when rotating at high speeds, so the impact of unbalanced masses cannot be ignored. The expression of the centrifugal force produced by the unbalanced mass is

$$F_c = m\omega^2 e, \tag{8}$$

where m denotes the unbalanced mass and ω denotes the speed of the rotor.

Since the length of spindle is short and the stiffness is high, the influence of bearing stiffness on the operation of the motorized spindle can be ignored, and the four-degree-of-freedom rotor model shown in Figure 3 is used, where (x, y, θ_x, θ_y) are the degrees of freedom, x and y are the lateral displacement and longitudinal displacement of the geometric center of the rotor, respectively, and (θ_x, θ_y) are the corner of the disc. A rotor with a disc not in the middle of the spindle will generate gyroscopic torque when the rotor rotates. Therefore, the influence of gyro torque cannot be ignored. The angle between the axis of the disc and the connecting line AB at both ends of the rotor is φ, the rotational angular velocity of the rotor is Ω, the rotor moment of inertia is J_d, and the polar moment of inertia is $J_p = 2J_d$. The momentum moment of the rotor is

$$H = J_p\Omega = 2J_d\Omega \tag{9}$$

Suppose that the plane formed by the axis of the disc and the connection AB has an angular velocity ω_n. Because the momentum moment of the precession disc H will constantly change direction, there is a moment of inertia

$$\vec{M} = -(\omega_n \times H) = H \times \omega_n = J_p\Omega \times \omega_n. \tag{10}$$

The direction is perpendicular to $O'AB$, and the size is

$$\vec{M} = -(\omega_n \times H) = H \times \omega_n = J_p\Omega\omega_n \sin\phi. \tag{11}$$

This moment is called the gyro moment or turning moment. It is the moment of the disc acting on the spindle. Because φ is smaller, $\sin\varphi \approx \varphi$. The above formula can be written as

$$\vec{M} = J_p\Omega\omega_n\varphi. \tag{12}$$

The dynamic differential equations of the motorized spindle rotor are derived based on Lagrange method. Lagrange's equation is

$$\frac{\mathrm{d}}{\mathrm{d}t}\left(\frac{\partial T}{\partial \dot{q}_j}\right) - \frac{\partial T}{\partial q_j} = Q_j, \quad j = 1, 2, \ldots, n. \tag{13}$$

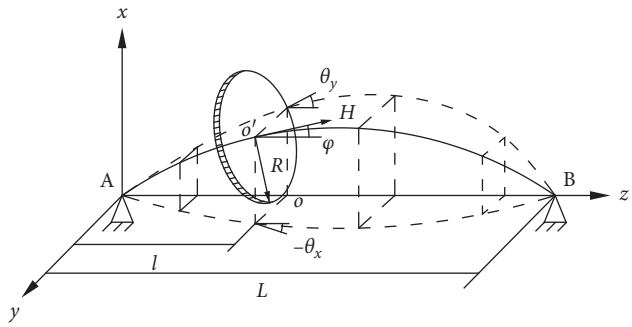

Figure 3: Schematic diagram of a 4-DOF rotor.

Let the coordinates of the center of gravity be

$$\begin{cases} x_G = x + e\cdot\cos\varphi, \\ y_G = y + e\cdot\sin\varphi, \end{cases} \tag{14}$$

where (x, y) denotes the coordinate of the geometric center of the rotor.

The kinetic energy of the rotor can be calculated by

$$T = \frac{m}{2}\left(\dot{x}_G^2 + \dot{y}_G^2\right) + \frac{1}{2}\left[J_d\left(\dot{\theta}_x^2 + \dot{\theta}_y^2\right) + J_p\Omega^2 - 2J_p\Omega^2\dot{\theta}_y\theta_x\right]. \tag{15}$$

Let the generalized coordinates be $q_1 = x$, $q_2 = y$, and $q_4 = \theta_y$, and the generalized force can be calculated by

$$\begin{cases} Q_1 = -k_{11}x - k_{14}\theta_y - c_{11}\dot{x} + F_x, \\ Q_2 = -k_{11}x + k_{14}\theta_y - c_{11}\dot{y} + F_y, \\ Q_3 = k_{14}y - k_{11}\theta_x - c_{33}\dot{\theta}_x, \\ Q_4 = -k_{14}x - k_{11}\theta_y - c_{33}\dot{\theta}_y. \end{cases} \tag{16}$$

The dynamic differential equation of the rotor is obtained by substituting equations (14)–(16) in equation (13):

$$\begin{cases} m\ddot{x} + c_{11}\dot{x} + k_{11}x + k_{14}\theta_y = me\Omega^2\cos\Omega t + F_x, \\ m\ddot{y} + c_{11}\dot{y} + k_{11}y - k_{14}\theta_x = me\Omega^2\sin\Omega t + F_y, \\ J_d\ddot{\theta}_x + H\dot{\theta}_y + c_{33}\dot{\theta}_x - k_{14}y + k_{33}\theta_x = o, \\ J_d\ddot{\theta}_y - H\dot{\theta}_x + c_{33}\dot{\theta}_y + k_{14}x + k_{33}\theta_y = o. \end{cases} \tag{17}$$

In the equation, m denotes the mass of the disk, e denotes the eccentricity distance of the mass, and k_{11} denotes the force applied at o' point when the center of the disk has a unit displacement in the x direction. k_{14} denotes the force applied at a point o' along y direction when unit rotation angle is available on axis $o'y$. k_{33} refers to the force applied at a point along x direction when there is a unit rotation angle around the axis $o'x$. c_{11} is the damping of point o' when it has a displacement in the x direction, and c_{33} is the damping of point o' when it has a turn around the x-axis.

3. Analysis of Unbalanced Vibration Characteristics of the Eccentric Motorized Spindle

The dynamic model of eccentric mass and unbalanced magnetic pull coupling fault motorized spindle is established by Lagrange method and solved numerically by the fourth-order Runge-Kutta method based on MATLAB. In the established model system, the effects of relative eccentricity on unbalanced magnetic pull, mass eccentricity e and static eccentricity r on axis track, and unbalanced vibration are analyzed, respectively. Vibration response law is obtained by processing parameters such as rotating speed v, mass eccentricity e, and static eccentricity r. Vibration characteristics of motorized spindle under mass eccentricity and air gap eccentricity are further understood through analysis results. The customized HT-170-20000-11 eccentric motorized spindle is used as the research object. Table 1 gives some parameters of the motorized spindle. For comparison, the static eccentric angle of the rotor is set to $\gamma = (\pi/4)$.

Table 1: Structural parameters of motorized spindle.

Parameter	Size
Spindle length	$L = 0.26$m
Material elastic modulus	$E = 2.1 \times 10^{11}$ (N/m^2)
Material density	$\rho = 7.85 \times 10^3$ (kg/m^3)
Rotor disc thickness	$T = 0.13$ m
Rotor radius	$R = 0.04$ m
Air gap width	$\delta_0 = 0.003$ m
Number of motor pole pairs	$p = 6$

3.1. Effect of Relative Eccentricity on Unbalanced Magnetic Pull. The relationship between relative eccentricity and air gap permeability coefficient is given in Figure 4. From the figure, it can be seen that the relative eccentricity and the air gap permeability coefficient are nonlinear. As the relative eccentricity increases, the air gap permeability coefficient also increases; and the increase rate is becoming faster and faster when the relative eccentricity is getting closer and closer to 1, because the air gap on one side of the rotor is close to infinity, which causes the magnetic pull on one side to rise sharply.

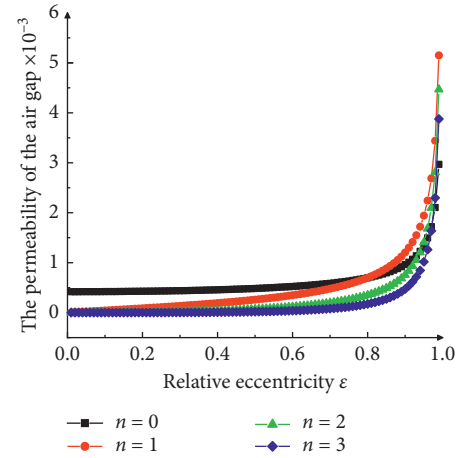

Figure 4: The relation between relative eccentricity and air gap permeability coefficient.

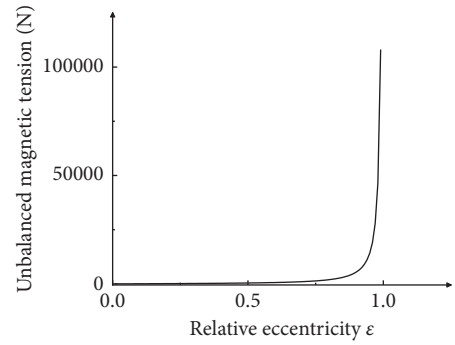

Figure 5: The relationship between relative eccentricity and magnetic force of gas unbalance.

From Figure 5, it can be concluded that when the relative eccentricity is less than 0.7, the unbalanced magnetic pull and the relative eccentricity are roughly linear, but when the relative eccentricity is close to 1, the unbalanced magnetic pull rises sharply and appears infinite, which is related to the increase of air gap permeability coefficient. The air gap permeability coefficient increases sharply when the relative eccentricity is close to 1, which increases the unbalanced magnetic pull to infinity. It will cause serious vibration of the motorized spindle and affect the stable operation of the motorized spindle.

3.2. Vibration Analysis in Time and Frequency Domains. Figures 6 and 7 are the frequency-domain and time-domain waveform diagrams of the motorized spindle at 6000 r/min and 12000 r/min, and the mass eccentricity is 5 μm. The static eccentricity is 0 μm, 30 μm, and 100 μm. When the static eccentricity in the frequency-domain diagram is 0 μm, the frequency-domain diagram has a peak at 100 Hz, and when the static eccentricity is added, a peak appears at about 0 Hz. This part of the peak value is caused by unbalanced magnetic pull, which is a manifestation of the effect of unbalanced magnetic pull on the vibration of motorized spindle. When the speed increases by 12000 r/min, the main peak position moves to about 200 Hz, and the peak value increases. To compare the two time-domain diagrams, it can be concluded that, with the appearance of static eccentricity, the initial phase of unbalanced vibration increases, and the amplitude of unbalanced vibration decreases in the positive direction and increases in the negative direction. This is consistent with the analysis results of the axis trajectory. With the increase of rotating speed, the time-domain diagrams coincide, and the effect of unbalanced magnetic pull weakens. Mass eccentricity becomes the main interfering factor.

3.3. Axis Track Analysis. Figure 8 shows the simulation axis track under the condition of rotating speed of 5000 r/min, mass eccentricity of 0.0001 m, and static eccentricity of

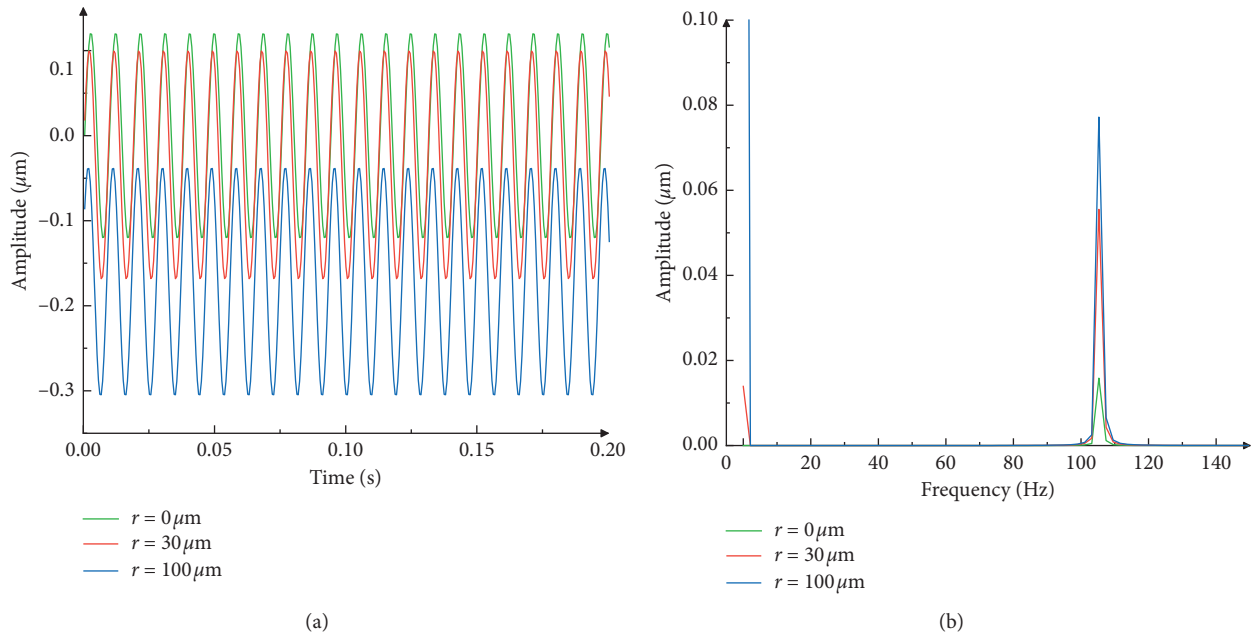

Figure 6: Time-domain and frequency-domain waveforms with mass eccentricity of 5 μm at 6000 r/min and different air gap eccentricity. (a) Time domain. (b) Frequency domain.

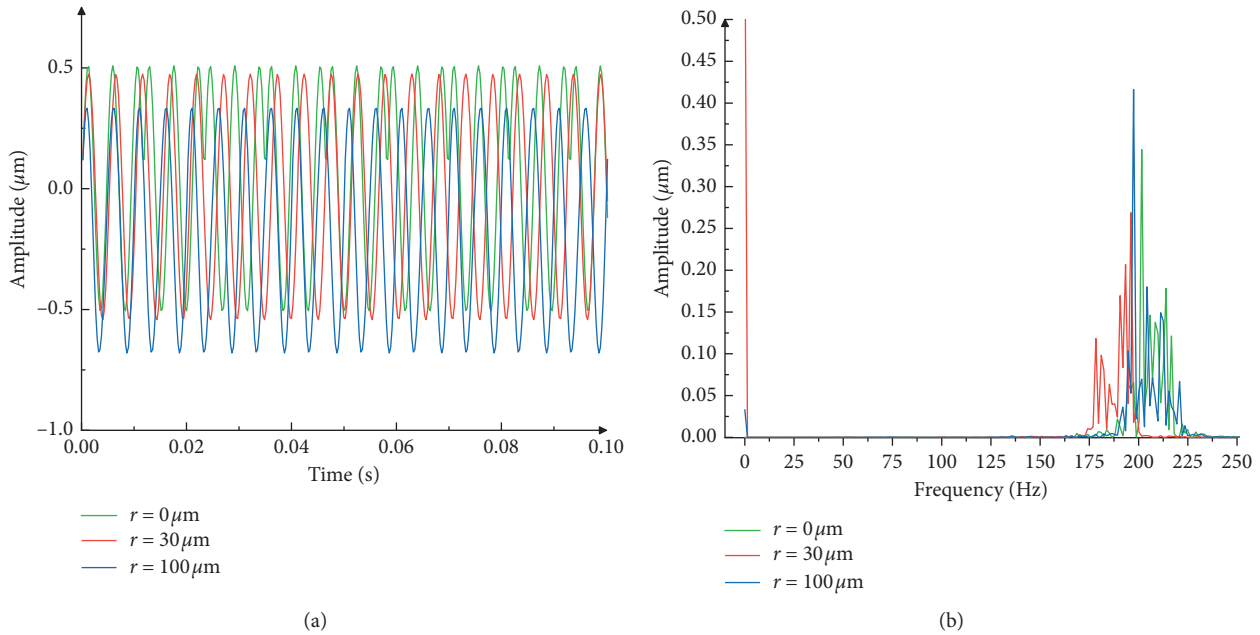

Figure 7: Time-domain and frequency-domain waveforms with the rotating speed of 12000 r/min, mass eccentricity of 5 μm, and different air gap eccentricity. (a) Time domain. (b) Frequency domain.

0.0001 m. Vibration occurred within a certain range, and the unbalanced magnetic pull changed the motion state of the motorized spindle rotor. By comparing Figure 8(b) with static eccentricity occurring at 45° and Figure 8(c) with static eccentricity occurring at 225°, it can be seen that when static eccentricity occurs at 45°, the axis trajectory shifts to the lower left. But when the eccentricity occurs at the position of 225°, the axis track shifts to the upper right, which shows that the unbalanced magnetic pull pushes the rotor to the side with larger air gap.

3.4. Vibration Analysis without Static Eccentricity. The rotor static eccentric distance r is set to zero. The amplitude along the X direction of the rotor is analyzed when the rotating speed increases under three unbalanced conditions: mass

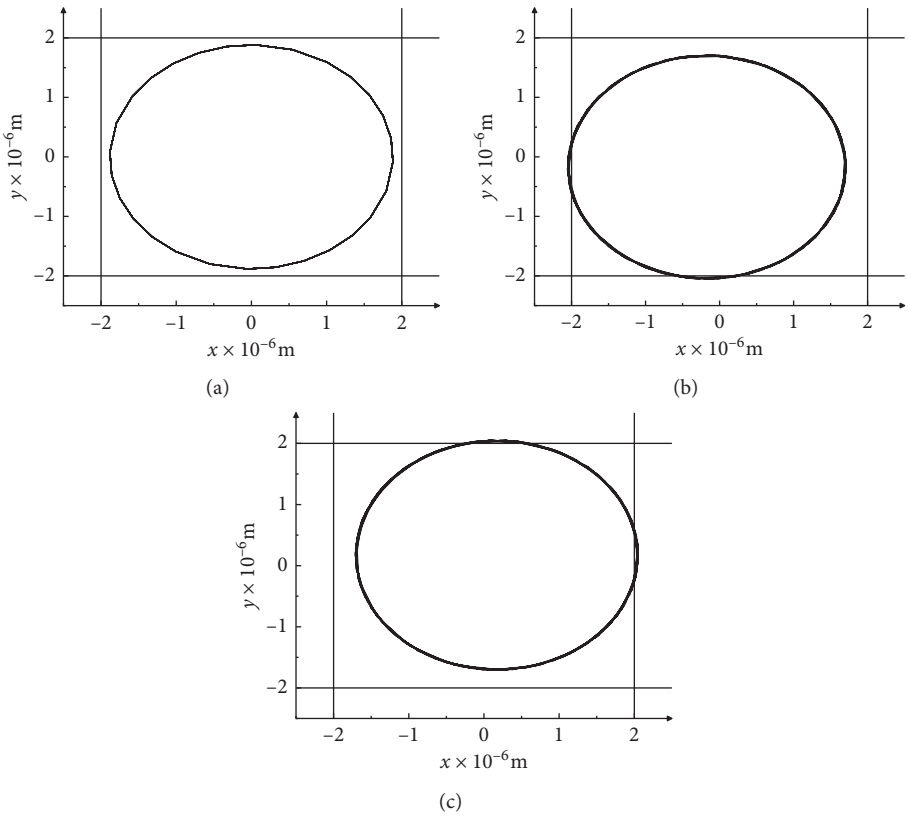

Figure 8: Orbit of spindle center. (a) No static eccentricity. (b) Static eccentricity at 45°. (c) Static eccentricity at 225°.

eccentricity e is 5 micron, 10 micron, and 15 micron, respectively. It can be concluded from Figure 9 that when the mass eccentricity is constant, the amplitude of the motorized spindle rotor increases with the increase of the speed, and the higher the speed is, the greater the amplitude of the unbalanced amplitude is. At the same speed, as the mass eccentricity increases, amplitude also increases, and the higher the speed is, the greater the amplitude of unbalanced vibration is. This is because the unbalanced force produced by the unbalanced mass has a square relationship with the speed, and the slope will gradually increase.

When the rotor static eccentric distance r is zero and the rotating speed is 10000 r/min and 20000 r/min, the variation of the amplitude of unbalanced vibration of motorized spindle with the increase of mass eccentricity is obtained. Figure 10 shows that the amplitude of the unbalanced vibration increases linearly with the increase of the mass eccentricity at the same speed, and, under the same mass eccentricity, the amplitude increases with the increase of the speed, and the higher the speed is, the greater the amplitude of unbalanced vibration is. This is also consistent with the model: the mass eccentricity and the unbalanced force produced by the eccentric mass have a linear relationship.

3.5. Effect of Static Eccentricity on Unbalanced Vibration. Effect of different mass eccentricity and static eccentricity on unbalanced vibration of motorized spindle is analyzed.

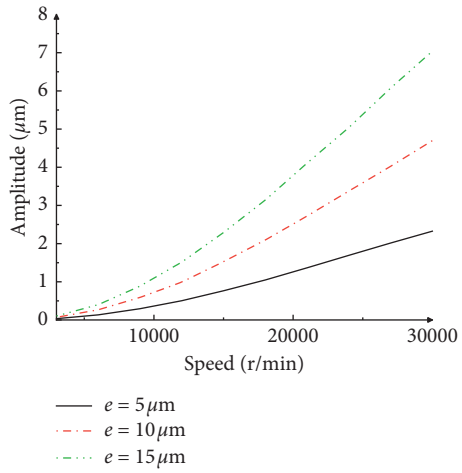

Figure 9: Effect of mass eccentricity on amplitude without static eccentricity.

Figure 11 shows that the vibration of the motorized spindle increases with the increase of the speed under the same static and mass eccentricity, and the increase of unbalanced vibration shows an upward trend, and the higher the rotating speed is, the greater the amplitude increase is. With the increase of unbalanced magnetic pull and static eccentricity, the vibration also increases. The three figures show that the

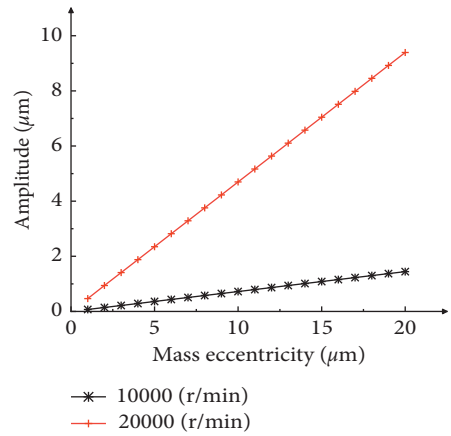

Figure 10: Effect of mass eccentricity on vibration without static eccentricity.

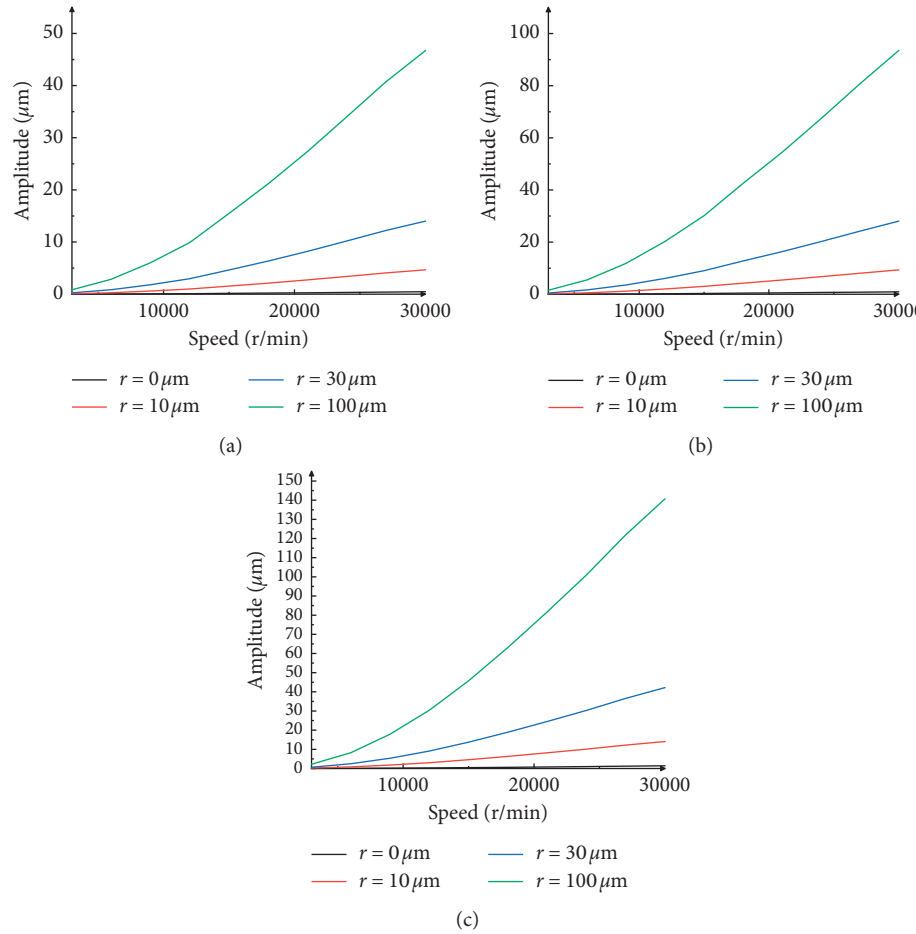

Figure 11: Effect of different static eccentricity on vibration with mass eccentricity of (a) 10 μm, (b) 20 μm, and (c) 30 μm.

unbalanced vibration increases as the mass eccentricity increases.

The change of unbalanced vibration with the increase of rotor static eccentricity under different mass eccentricity at speeds of 5000 r/min and 30000 r/min is analyzed. The vibration increases as the static eccentricity of the motorized spindle increases linearly, as shown in Figure 12. Under the same speed and static eccentricity, the amplitude of unbalanced vibration increases with the mass eccentricity.

The increase of unbalanced vibration with mass eccentricity under the same static eccentricity is analyzed when the rotating speed is 5000 r/min and 10000 r/min. At the same speed and static eccentricity of the rotor, as the mass eccentricity increases, the unbalanced vibration increases

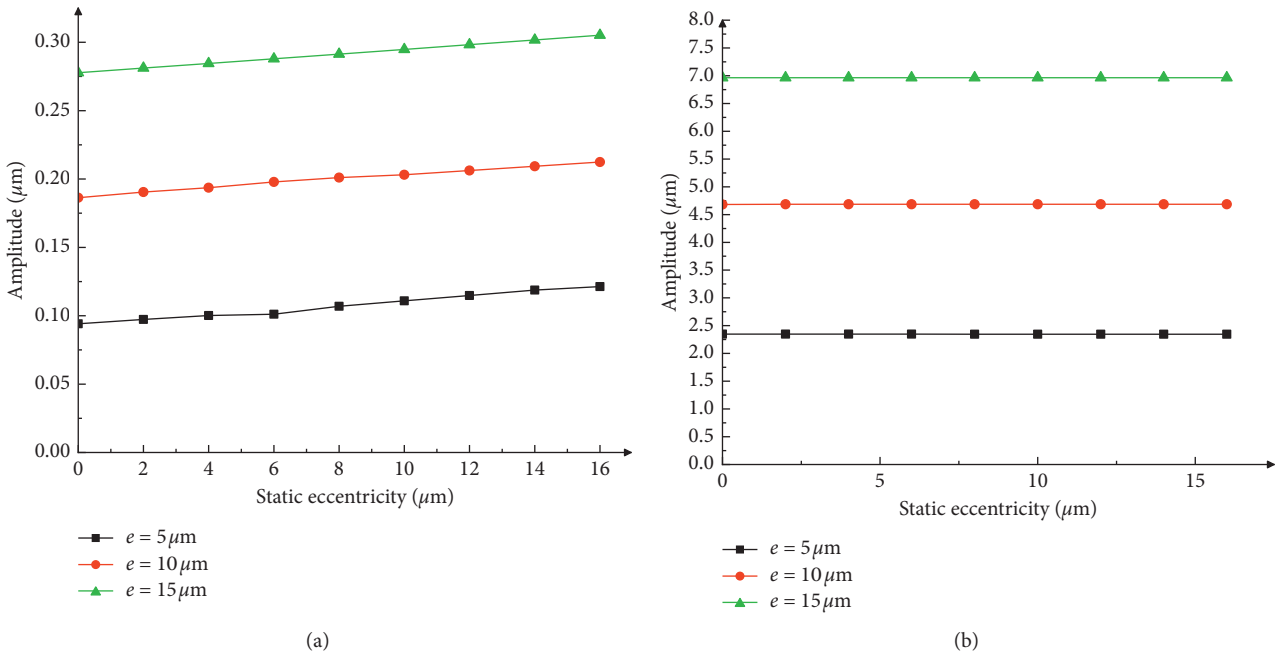

Figure 12: Effect of static eccentricity on vibration under different mass eccentricity at (a) 5000 r/min and (b) 30000 r/min.

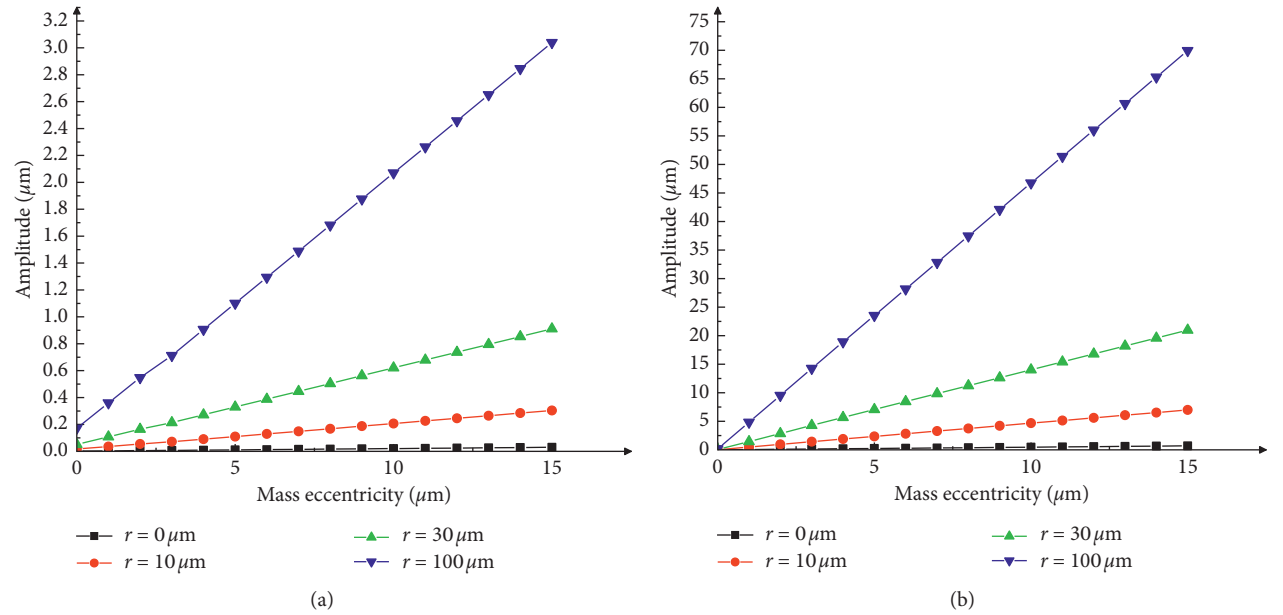

Figure 13: Effect of mass eccentricity on vibration at the rotating speed of (a) 5000 r/min and (b) 30000 r/min.

and rises linearly, as shown in Figure 13. Under the same mass eccentricity and speed, the unbalanced vibration amplitude increases with static eccentricity.

The effect of unbalanced tension on the vibration of the motorized spindle rotor is calculated when there is no mass eccentricity in the motorized spindle. In Figure 14, r is the static eccentricity of the rotor spindle, and the unbalanced magnetic pull is proportional to the static eccentricity. Figure 14 shows that the influence of unbalanced magnetic pull on unbalanced vibration has nothing to do with the speed and only depends on the size of the static eccentricity of the rotor spindle, which increases with the increase of the static eccentricity.

4. Experimental Verification

The experiment uses the motorized spindle test platform shown in Figure 15 for experimental verification. The motorized spindle is two customized HT-170-20000-11 eccentric motorized spindles with air gap eccentricity of

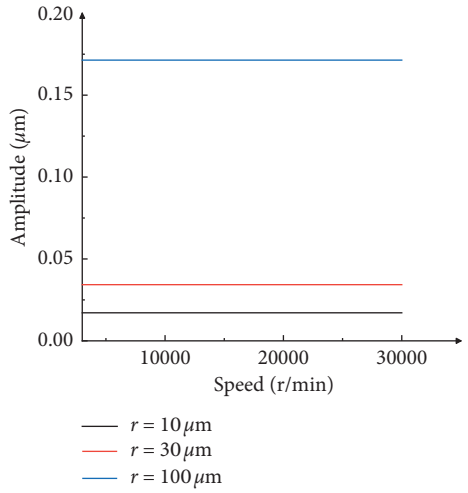

Figure 14: Effect of different static eccentricity on vibration with the increase of rotating speed.

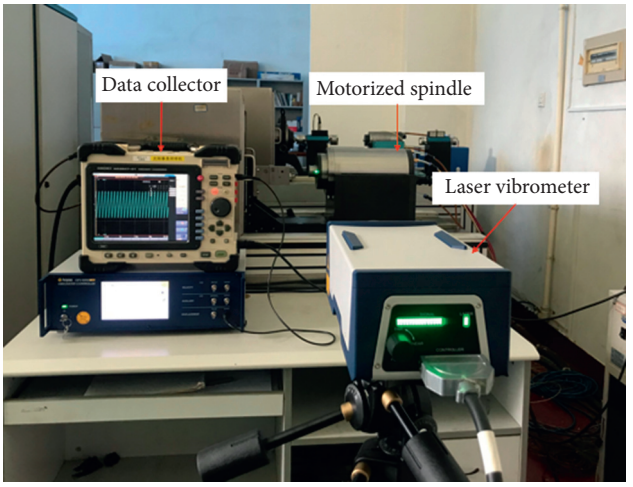

Figure 15: Motorized spindle test platform.

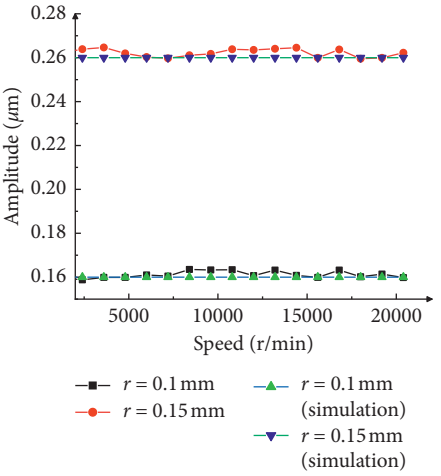

Figure 16: Comparison between simulation and experiment.

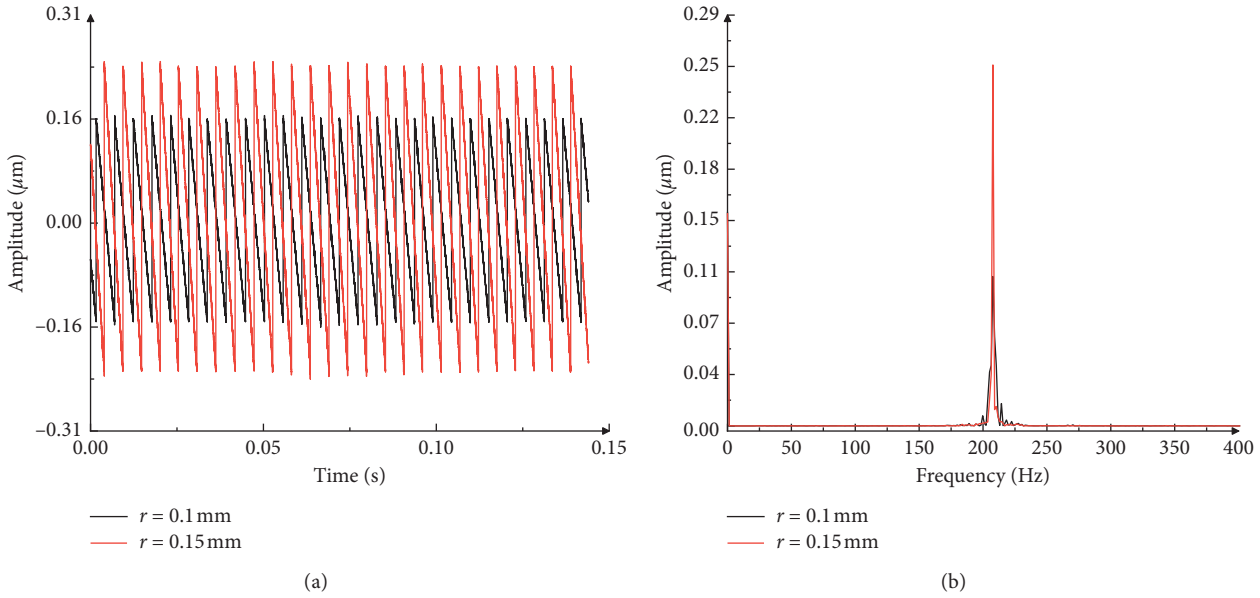

Figure 17: Time-domain and frequency-domain waveforms with the rotating speed of 12000 r/min. (a) Time domain. (b) Frequency domain.

0.1 mm and 0.15 mm. In the experiment, a laser vibrometer of Germany's Polytec GmbH company model OFV-50555000 Xtra is used to measure the unbalanced vibration of the motorized spindle during operation. Because of the limitation of actual experimental conditions, the experiment mainly reflects the vibration of the rotor by monitoring the exposed rotating spindle at the end of the motorized spindle. The data display instrument is used to export the experimental data.

The experiment uses 0.1 mm and 0.15 mm static eccentric HT-170-20000-11 motorized spindles and carries out the vibration experiment of the motorized spindle with increasing speed. Through the experiment, it can be concluded that the vibration caused by the static eccentricity of the motorized spindle fluctuates in a certain small range with the increase of the speed, but it can be regarded as basically unchanged because of the more external influence. As the static eccentricity increases, the unbalanced vibration will increase. This matches the simulation result. Figure 16 shows the comparison between simulation and experiment under different static eccentricity. Through comparison, the experiment and simulation are roughly consistent within a small range, and the model has a high accuracy.

Figure 17 shows the time-domain waveform diagrams and frequency-domain diagrams of the motorized spindle at 12000 r/min obtained from the experiment. When the static eccentricity increases, the amplitude of the unbalanced vibration also increases with it. In the frequency-domain diagram, since the motorized spindle has a slight mass eccentricity, a peak appears in the fundamental frequency. When the static eccentricity increases, the amplitude of the unbalanced vibration also increases. Because of the static eccentricity, peak value appears at 0 Hz, which is consistent with the simulation results.

5. Conclusions

The mechanism of unbalanced magnetic pull force is analyzed, and the influence of gyroscopic moment is considered. A dynamic model of eccentric mass and unbalanced magnetic pull coupling fault motorized spindle is established by Lagrange method. Through the simulation analysis of the model and the comparison with the experiment, the influence of unbalanced magnetic pull on unbalanced vibration of the spindle does not increase with the speed of the spindle but is only related to the eccentric distance. The larger the eccentric distance is, the greater the vibration will be. When the relative eccentricity approaches 1, an infinite unbalanced magnetic pull will occur, and the unbalanced vibration of the rotor will deviate to the direction of large air gap. When there is mass eccentricity, the amplitude of unbalanced vibration increases with the increase of speed. When the speed is constant, the amplitude increases linearly with the increase of mass eccentricity. Through the above analysis, the coupling dynamic behavior of eccentric faulted motorized spindle under the influence of unbalanced magnetic pull is revealed.

Data Availability

The data used to support the findings of this study are included within the article.

Conflicts of Interest

The authors declare that they have no conflicts of interest.

Acknowledgments

This work was supported by the National Natural Science Foundation of China (Grant no. 51805337), the Key

Laboratory of Vibration and Control of Aero-Propulsion System, Ministry of Education, Northeastern University (Grant no. VCAME202008), and the Scientific Research Project of Liaoning Provincial Education Department (Grant no. lnjc202010).

References

[1] J. Liu, T. Lai, and X. Chen, "Dynamics analysis of unbalanced motorized spindles supported on ball bearings," *Shock and Vibration*, vol. 2016, Article ID 2787524, 10 pages, 2016.

[2] H. Shi, Y. Li, X. Bai et al., "Investigation of the orbit-spinning behaviors of the outer ring in a full ceramic ball bearing-steel pedestal system in wide temperature ranges," *Mechanical Systems and Signal Processing*, vol. 149, Article ID 107317, 2021.

[3] M. Hou and H. Shi, "Stator-winding incipient shorted-turn fault detection for motor system in motorized spindle using modified interval observers," *IEEE Transactions on Instrumentation and Measurement*, vol. 70, pp. 1–16, 2020.

[4] W. Shan, X. Chen, H. Wang, and C. Yu, "Milling stability of high speed motorized spindles," *Journal of Vibration and Shock*, vol. 36, no. 19, pp. 242–249, 2017.

[5] H. P. Phadatare and B. Pratiher, "Nonlinear modeling, dynamics, and chaos in a large deflection model of a rotor-disk-bearing system under geometric eccentricity and mass unbalance," *Acta Mechanica*, vol. 231, no. 3, pp. 907–928, 2020.

[6] N. Wang and D. Jiang, "Vibration response characteristics of a dual-rotor with unbalance-misalignment coupling faults: theoretical analysis and experimental study," *Mechanism and Machine Theory*, vol. 125, pp. 207–219, 2018.

[7] X. Qiao and C. Zhu, "Experimental study on controlling actively wheel unbalance vibration," *Journal of Vibration Engineering*, vol. 30, no. 1, pp. 55–61, 2017.

[8] S. Bab, S. E. Khadem, A. Abbasi, and M. Shahgholi, "Dynamic stability and nonlinear vibration analysis of a rotor system with flexible/rigid blades," *Mechanism and Machine Theory*, vol. 105, pp. 633–653, 2016.

[9] E. Yue, C. Gan, and S. Yang, "Vibration characteristics analysis of a rotor for a permanent magnet motor with Air-Gap Eccentricity," *Journal of Vibration and Shock*, vol. 33, no. 8, pp. 29–34, 2014.

[10] X. Kong, J. Niu, Y. Luo, and Q. Xu, "Sommerfeld effect and unbalanced response analysis in single disk rotor system with eccentric mass considering induction motor model," *Journal of Mechanical Engineering*, vol. 56, no. 17, pp. 137–144, 2020.

[11] F. Gao, M. Cheng, Y. Li, W. Jia, and P. He, "Eccentric vibration analysis and test of permanent magnet synchronous grinding motorized spindle," *Chinese Journal of Scientific Instrument*, vol. 40, no. 2, pp. 38–50, 2019.

[12] J. Faiz, M. Hassanzadeh, and A. Kiyoumarsi, "Analytical calculation of magnetic field in surface-mounted permanent-magnet machines with air-gap eccentricity," *COMPEL-The International Journal for Computation and Mathematics in Electrical and Electronic Engineering*, vol. 38, no. 2, pp. 893–914, 2019.

[13] X. Xu, Q. Han, and F. Chu, "A four degrees-of-freedom model for a misaligned electrical rotor," *Journal of Sound and Vibration*, vol. 358, pp. 356–374, 2015.

[14] G.-J. Tang, Y.-L. He, S.-T. Wan, and L. Xiang, "Investigation on stator vibration characteristics under air-gap eccentricity and rotor short circuit composite faults," *Journal of the Brazilian Society of Mechanical Sciences and Engineering*, vol. 36, no. 3, pp. 511–522, 2014.

[15] S. Zuo, D. Li, Y. Mao, and W. Deng, "Longitudinal vibration analysis and suppression of electric wheel system driven by in-wheel motor considering unbalanced magnetic pull," *Proceedings of the Institution of Mechanical Engineers, Part D: Journal of Automobile Engineering*, vol. 233, no. 11, pp. 2729–2745, 2019.

[16] H. Liu, Y. Wu, X. Wang, P. Yan, and X. Zhang, "Nonlinear normal modes and primary resonance for permanent magnet synchronous motors with a nonlinear restoring force and an unbalanced magnetic pull," *Nonlinear Dynamics*, vol. 97, no. 2, pp. 1197–1213, 2019.

[17] F. Boy and H. Hetzler, "Rotordynamics of two-Pole turbo generators with refined modelling of the unbalanced magnetic pull," *PAMM*, vol. 15, no. 1, pp. 243-244, 2015.

[18] F. Liu, C. Xiang, H. Liu et al., "Asymmetric effect of static radial eccentricity on the vibration characteristics of the rotor system of permanent magnet synchronous motors in electric vehicles," *Nonlinear Dynamics*, vol. 96, no. 4, pp. 2581–2600, 2019.

[19] F. Liu, H. Liu, C. Xiang et al., "Influence of unbalanced magnetic pull on free vibration characteristics of motor rotor based on multi-scale method," *Journal of Mechanical Engineering*, vol. 53, no. 16, pp. 52–60, 2017.

[20] G. Kumar and K. Kalita, "Vibration control using bcw induction motor, Procedia Engineering," *Indian Institute of Technology Guwahati*, vol. 144, no. 2, pp. 94–101, 2016.

[21] X. Chen, P. Zhang, J. Liu, and Y. He, "Multi-physical coupled dynamic characteristics of high-speed motorized spindles," *Journal of Vibration Engineering*, vol. 26, no. 3, pp. 303–310, 2013.

[22] C. Xiang, F. Liu, H. Liu, L. Han, and X. Zhang, "Nonlinear dynamic behaviors of permanent magnet synchronous motors in electric vehicles caused by unbalanced magnetic pull," *Journal of Sound and Vibration*, vol. 371, pp. 277–294, 2016.

[23] J. Tang, W. Deng, and Y. He, "Effect of different kinds of air-gap eccentricity faults on rotor UMP of a turbo-generator," *Journal of Vibration and Shock*, vol. 36, no. 15, pp. 1–8, 2017.

[24] U. Werner, "Influence of electromagnetic field damping on forced vibrations of induction rotors caused by dynamic rotor eccentricity," *ZAMM-Journal of Applied Mathematics and Mechanics/Zeitschrift für Angewandte Mathematik und Mechanik*, vol. 97, no. 1, pp. 38–59, 2017.